Scripta Materialia 152 (2018) 59–63

Contents lists available at ScienceDirect

Scripta Materialia

journal homepage: www.elsevier.com/locate/scriptamat

Regular article

The interaction between Mn and Fe on the precipitation of Mn/Fe dispersoids in Al-Mg-Si-Mn-Fe alloys

C.L. Liu [a], Q. Du [b], N.C. Parson [c], W.J. Poole [a,*]

[a] Department of Materials Engineering, The University of British Columbia, Vancouver, Canada
[b] SINTEF Materials and Chemistry, Trondheim, Norway
[c] Rio Tinto Aluminium, Jonquiere, Canada

ARTICLE INFO

Article history:
Received 8 January 2018
Received in revised form 8 April 2018
Accepted 8 April 2018
Available online xxxx

Keywords:
Al-Mg-Si-Mn-Fe alloys
Homogenization
Dispersoids

ABSTRACT

The formation of Mn/Fe containing precipitates during a high temperature treatment known as homogenization is important for the downstream performance of 6XXX aluminum extrusion alloys. In this work, the complex interaction between Mn and Fe during precipitation has been studied using a combination of experiments and a model that includes long range diffusion of Fe and Mn and a short range precipitation model. The results reveal the unusual phenomenon where Fe first diffuses from the constituent particles to the dispersoids, thereby increasing their volume fraction, and then at longer times reverses direction to diffuse back to the constituent particles.

There is currently a significant scientific and industrial interest in the use of Al-Mg-Si-Mn-Fe extrusion alloys in automotive applications to reduce the weight of vehicles. The production of aluminum extrusion alloys involves many steps starting with direct chill casting of billets followed by a high temperature heat treatment (550–580 °C for 4–24 h) known as homogenization. The objective of the homogenization treatment is to modify the as-cast microstructure by: i) reducing segregation of Mg and Si [1], ii) dissolving Mg_2Si precipitates [2], iii) spherodizing the constituent particles [3] and iv) precipitating Mn/Fe bearing particles known as dispersoids [4]. This work is concerned with the precipitation of dispersoids with sizes of 20 to 100 nm which occurs over several hours during heating and the hold at the homogenization temperature. The radius and volume fraction of dispersoids plays an important role on the high temperature flow stress [5], the inhibition of recrystallization during and after extrusion (via Zener drag) [6] and the quench sensitivity of the alloys [7–9].

The nucleation of Mn/Fe containing dispersoids occurs during heating to the homogenization temperature. A complex precipitation path is observed with Mg-Si metastable precipitates first forming. These precipitates act as heterogeneous nucleation sites for Mn/Fe dispersoids and then dissolve as the solubility limit increases (e.g. see the seminal work of Lodgaard and Ryum [4]). The stoichiometry of the so called α-Al(MnFe)Si dispersoids has been observed to be variable but it is generally accepted that there are 138 atoms in the unit cell of dispersoids [10–12] with a composition of $Al_{100}(MnFe)_{24}Si_{14}$ [10,11] or $Al_{96}(MnFe)_{24}Si_{18}$ [12], where Mn and Fe can substitute for each other. The crystal structure of the dispersoids has been found to be either simple cubic (SC) or body centred cubic (bcc) with a lattice parameter of 1.25–1.26 nm [13,14].

The evolution of dispersoid size and number density during homogenization has been examined in a number of studies. The Alstruc homogenization model developed by the SINTEF group in Norway was an early attempt to model dispersoid evolution [15,16] for a wide range of chemistries. Later, Cai et al. developed a model to predict the solute distribution after solidification using a multicomponent Scheil model and then rationalized the spatial distribution of dispersoid precipitation based on the local chemical driving force [2]. Recently, Priya et al. developed a 2D finite volume-cellular automaton model to simulate microstructure changes at the secondary dendrite arm spacing (SDAS) length scale and 1D finite difference model for the precipitation of Mg_2Si during cooling [9]. In addition, Du et al. developed a CALPHAD based homogenization model to predict dispersoid evolution for quaternary Al-Mn-Fe-Si alloys [17]. Precipitation/dissolution of dispersoids is considered using a Kampmann-Wagner (KWN) size class based model which includes classical nucleation theory, diffusional growth and accounts for local compositional effects. Long range diffusion of Fe/Mn is accounted for using a finite volume method one-dimensional (1-D) pseudo front tracking (PFT) model. The two models interrogate a multicomponent CALPHAD database for local thermodynamic data and are tightly coupled to ensure a global mass balance is maintained in the system [17]. The model shows that the initial precipitation of dispersoids is spatially inhomogeneous due to the initial segregation of Mn after solidification and the formation of dispersoid free zones can be

* Corresponding author.
E-mail address: warren.poole@ubc.ca. (W.J. Poole).

https://doi.org/10.1016/j.scriptamat.2018.04.012
1359-6462/

rationalized by long range diffusion of Mn across the primary aluminum dendrite to the constituent particles.

The objective of the current work is to extend this analysis to examine the complex interplay between short and long range diffusion of Mn and Fe during high temperature homogenization heat treatment for a quinary alloy (Al-Mg-Si-Mn-Fe). It is of particular interest to examine the interaction between Mn and Fe and its effect on dispersoid formation during homogenization so as to allow for the design of new improved alloys and homogenization processes.

An Al-Mg-Si-Mn-Fe alloy was cast as extrusion billets (100 mm in diameter) by the Rio Tinto Aluminum Research and Development Center (ARDC) in Arvida, Quebec. The chemical composition of the alloy as measured by optical emission spectroscopy (OES) was: 0.71 wt% Mg, 1.03 wt% Si, 0.50 wt% Mn, 0.21 wt% Fe. Temperatures of 550 and 580 °C were chosen for the homogenization experiments, i.e. above the Mg_2Si solvus temperature and below the equilibrium melting temperature. An industrial heating rate of 200 °C/h was used and holding times of 0.17 h (10 min) and 2 h at 550 °C and 2, 12 and 168 h (7 days) at 580 °C were examined.

The secondary dendrite arm spacing (SDAS) was measured to be ≈20 μm. Dispersoid size distributions for each homogenization condition were quantified using back backscatter electron (BSE) images (Zeiss Sigma field emission gun scanning electron microscope) taken on polished samples. Fig. 1a shows an example for a sample homogenized for 12 h at 580 °C which shows the disperoids, the constituent particles and a dispersoid free zone (DFZ) around the constituent particles. The chemical composition of the dispersoids was analyzed by EDS using TEM thin foils, prepared by jet electro-polishing using a 30% nitric acid - 70% methanol electrolyte at −45 °C with a voltage of 15 V. The chemical composition of the dispersoids was conducted by energy dispersive (EDS) x-ray analysis using a JEOL 2010F TEM operating at 200 kV with the spot mode at the centre of the dispersoid; ≈ the Mn/Fe ratio for 30 dispersoids were characterized for each condition. Finally, Electron Probe Micro-Analysis (EPMA) was used to measure the distribution of Fe and Mn as a function of the homogenization conditions using a CAMECA SX-50. The accelerating voltage was 15 kV, the beam current was 20 nA and a beam size of ≈1 μm was used. The interaction volume was estimated to be 2 to 3 μm based on the CASINO Monte Carlo software [18]. The composition was measured based on three to five random lines of ≈250–300 μm in length using standards of a known composition [19]. The EPMA data was sorted from the lowest to highest Fe content as proposed by Gungor and Ganesan et al. [20,21] as shown in Fig. 1b. The examination of the data suggests that the measurements could be divided into two groups, low Fe and high Fe as, for this example, demarked by the distinct change in slope at 0.05 wt%. As such, the "low" Fe measurements have been associated with cases where the interaction volume for x-ray generation was entirely within the primary aluminum phase while the measurements with "high" Fe are related to situations where part of the interaction volume was within the constituent particles. For each homogenization condition, a normal distribution was fit to the measurements for Mn and Fe compositions.

Table 1 reports the evolution for the average radius and chemical composition (in terms of the average Mn/Fe ratio) of the dispersoids for different homogenization times/temperatures. It can be seen that, as expected, the dispersoid radius increases with temperature and time starting from 20 nm at the end of the heating ramp to 550 °C and coarsening to 98 nm after holding for 24 h at 580 °C. Fig. 1c shows a histogram for the Mn/Fe ratio measured by EDS in the TEM. Here, it can be observed that as the homogenization time/temperature is increased, the Mn/Fe ratio of the dispersoids decreases from ≈16 for the initial condition (i.e. quenching immediately after reaching a temperature of 550 °C during heating) to a value of ≈5 after heating and holding for 12 h at 580 °C.

Fig. 2a and b plot the compositional measurements in the primary aluminum phase from EPMA for Mn and Fe, respectively, for the different homogenization conditions. Here, as previously noted, the diameter of the interaction volume is ≈2–3 μm and as such, it is not possible to distinguish Mn or Fe in solid solution from the Mn or Fe in the dispersoids. Nevertheless, a number of interesting observations can be made

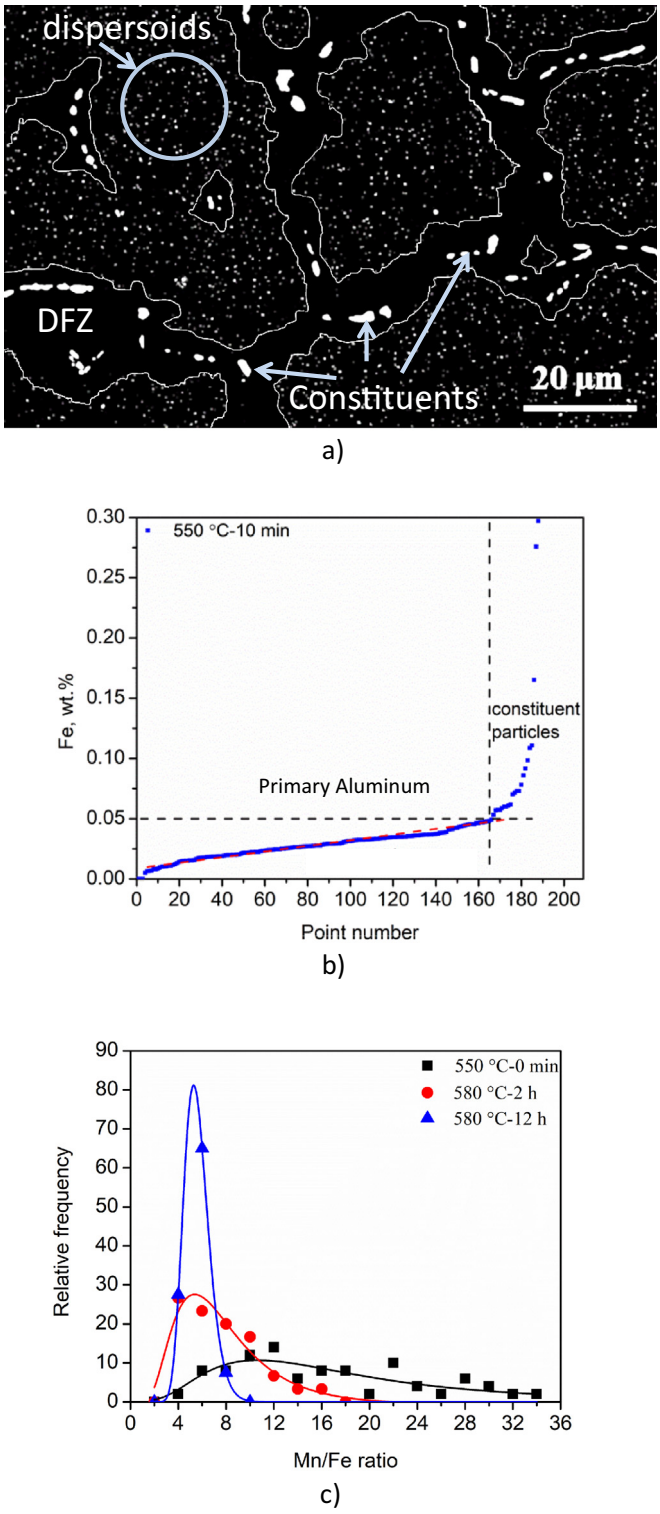

Fig. 1. a) an example of a backscatter electron image illustrating dispersoids, a dispersoid free zone (DFZ) and constituent particles (homogenization of 12 h at 580 °C, b) an example of electron probe microanalysis (EPMA) measurements showing the distribution of Fe composition measurements after sorting from smallest to largest (see text) and c) a histogram showing the Mn/Fe ratio of the dispersoids for different homogenization conditions as measured by EDS at the centre of the dispersoid using spot mode in the TEM.

Table 1
Experimental measurements of the equivalent area radius and the average Mn/Fe ratio at the centre of the dispersoid as measured by EDS using STEM in the spot mode. The mean radius and variance of the dispersoids were obtained from fitting a log normal distribution to the experimentally measured radii from the FEGSEM backscatter electron images.

	550 °C – 0 h	550 °C – 2 h	580 °C – 2 h	580 °C – 12 h	580 °C – 24 h
Mean radius (variance)/nm	20 (12)	40 (18)	56(31)	84 (29)	98 (30)
Mn/Fe ratio	16.3	16.4	6.6	4.6	–

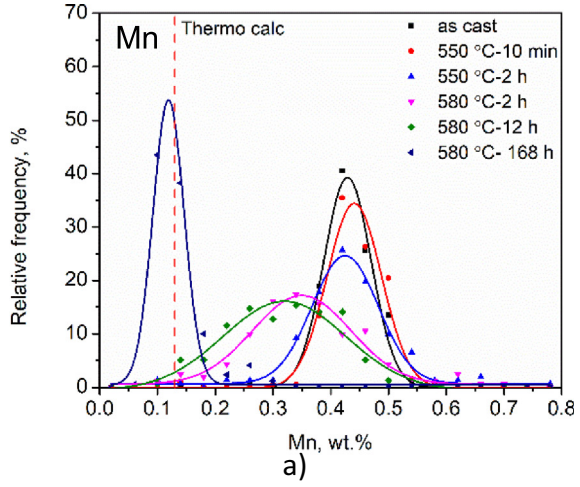

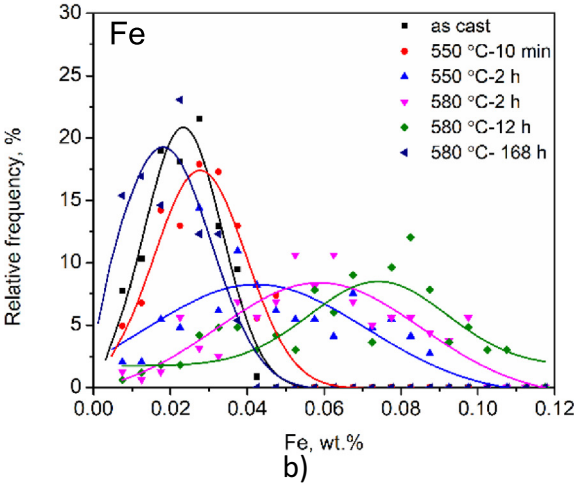

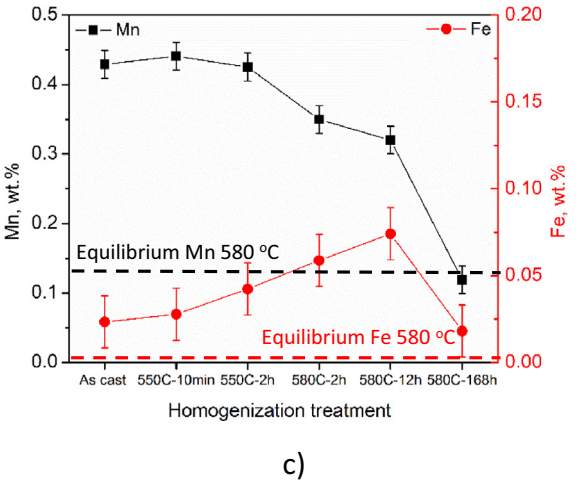

Fig. 2. Distributions for the composition in the primary aluminum phase from EPMA measurements for various homogenization conditions, a) for Mn and (b) for Fe and (c) the mean values for Mn and Fe compositional measurements as function of homogenization treatments.

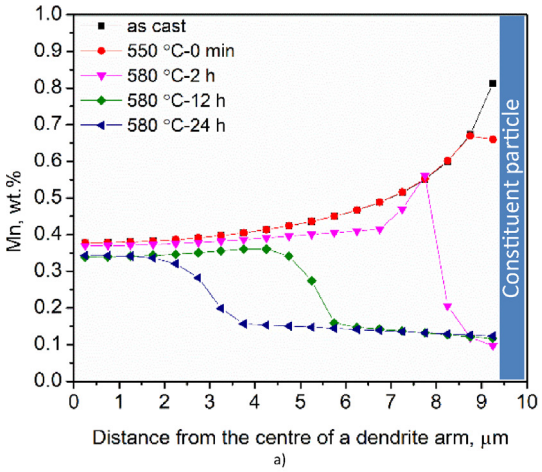

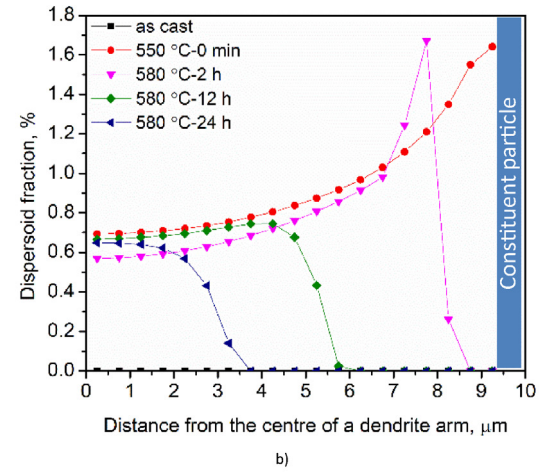

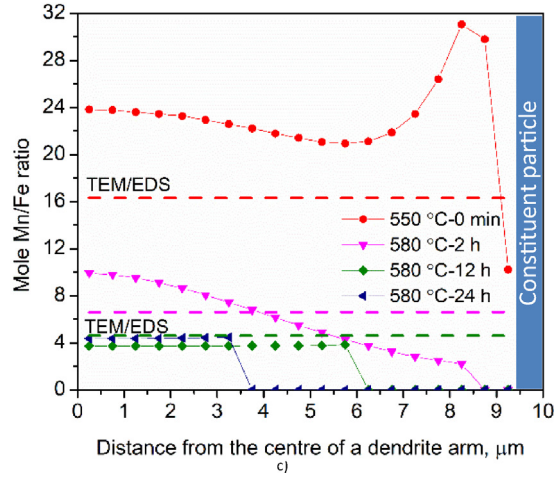

Fig. 3. Spatial distributions from the homogenization model for a) the total Mn content (i.e. sum of Mn in solid solution and in dispersoids), b) the volume fraction of dispersoids and c) the molar Mn/Fe ratio. Note, the left axis represents the centre of the dendrite and right axis is the constituent particles in the interdendritic region.

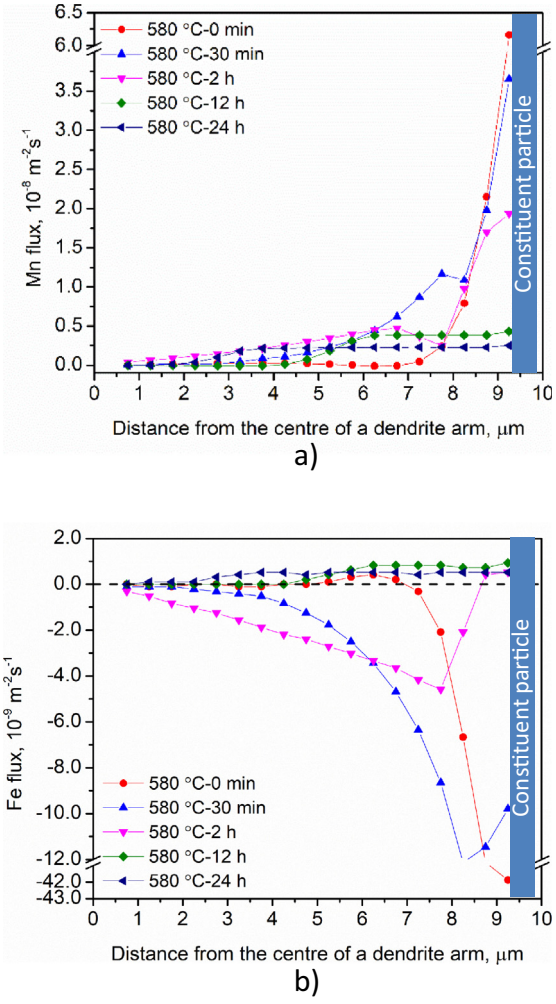

Fig. 4. Model results for: a) Mn flux and (b) Fe flux as a function of the position in the dendrite arm. Note: positive fluxes are for diffusion of the element from left to right and negative fluxes are for diffusion from right to left.

from these measurements. Starting with Fig. 2a for Mn, it can be observed that the data for the as-cast condition shows a mean value of 0.43 wt% Mn with a range of 0.35–0.55. The mean is lower than the bulk Mn level of 0.50 wt% due to the Mn in the constituent particles and the width of the distribution reflects the initial segregation of Mn. Optical microscope observations from samples etched with HF acid show no evidence of dispersoids suggesting the primary aluminum is supersaturated in Mn. Upon heating to 550 °C and holding for 10 min, there is almost no change in the Mn distribution. However, TEM observations show that precipitation of Mn/Fe dispersoids with an average radius of 20 nm has occurred (see results for 550 °C 0 h in Table 1). This would be consistent with there being insufficient time at 550 °C for significant long range diffusion of Mn, i.e. the average Mn spatial compositional variation is unchanged but now Mn is primarily in dispersoids rather than in solid solution. As the homogenization temperature and time is increased to 2 h at 580 °C, the width of the distribution widens. This is interpreted as a reflection of changes in the Mn profile due to long range diffusion of Mn. Upon further holding to 12 h at 580 °C, the distribution further widens. Finally, for a hold time of 168 h (7 days) at 580 °C, the system approaches equilibrium in which case the dispersoids are almost completely dissolved and Mn has diffused from within the primary aluminum phase to the constituent particles. Here, it can be seen that the average Mn concentration of 0.12 wt% in the primary aluminum phase measured by microprobe is close to the Thermocalc equilibrium prediction of 0.13 wt%.

Turning to the data for Fe, a different behaviour is observed. In Fig. 2b, it can be seen that the mean value for the as-cast sample is ≈0.02 wt% Fe and the distribution is relatively narrow. As the holding time/temperature increases to 2 h at 550 or 580 °C, the mean value increases to 0.04 and 0.06 wt% Fe, respectively, while the distribution widens considerably. The mean further increases after a treatment of 12 h at 580 °C to 0.075 wt% Fe but then decreases to ≈0.02 wt% Fe after holding for 168 h (1 week) at 580 °C. The evolution of the mean values for Mn and Fe concentrations in the primary aluminum phase as a function of homogenization condition is shown in Fig. 2c. Here, it can be observed that the Mn concentration continuously decreases with time and temperature until it approaches the equilibrium concentration after 168 h (1 week) at 580 °C. On the other hand, the Fe concentration first increases during homogenization reaching a maximum for the condition of 12 h at 580 °C after which it decreases to a low value. The low solubility of Fe in aluminum (0.0023 wt% at 580 °C) means that the solid solution contribution can be ignored, i.e. the measurement reflects Fe in the dispersoids. Thus, the increase in the Fe concentration relates to an increase in Fe content of the dispersoids and which would be consistent with the decrease in the Mn/Fe ratio of the dispersoids shown in in Fig. 1c or Table 1. The EPMA measurements are strong experimental evidence that Fe first diffuses from the constituent particles in the interdendritic region to the dispersoids (thereby decreasing their Fe/Mn ratio), and then later reverses direction to diffuse back to the constituent particles as the dispersoids dissolve following the long range diffusion of Mn.

To reveal the details of the Fe/Mn diffusion behaviour, the homogenization model of Du et al. for Al-Mn-Fe-Si alloys was modified (see references [17, 22, 23] for full details). This was accomplished by first updating the thermodynamic database with a new one for the Al-Mg-Si-Mn-Fe system and then calibrating the model for the density of nucleation sites and the interfacial energy of the matrix-dispersoid interface by a trial and error process. A good fit to the experimental data for dispersoid radius was found with the number of nucleation sites per volume = 100/μm^3 and an interfacial energy of 150 mJ/m^2. The length of the diffusion domain was discretized into 20 steps and was set as ½ the SDAS (i.e. 10 μm). Fig. 3 shows the results from the simulation where the heating rate was 200 °C/h and followed by holding at 580 °C. Fig. 3a shows the total Mn concentration (i.e. the sum of Mn in dispersoids and in solid solution) for the different homogenization conditions. For the as-cast case, it can be seen that there is a gradient of Mn from the centre of the dendrite (far left) to the interdendritic region (far right) reflecting the segregation from the solidification simulation. Fig. 3b shows that the dendrite is initially supersaturated in Mn, i.e. the volume fraction of dispersoids = 0. Upon heating to 550 °C, the Mn comes out of solution as Mn/Fe bearing dispersoids and the volume

Table 2
Summary of experimental measurements and model predictions for the volume fraction and composition (in terms of Mn/Fe ratio) for the evolution of constituent particles during homogenization at 580 °C. The experimental measurements of volume fraction were determined by image analysis and the Mn/Fe ratio calculated from the EPMA measurements on the data associated with the constituent particles.

	Volume fraction (experimental)/%	Volume fraction (simulation)/%	Mn/Fe ratio (experimental)	Mn/Fe ratio (simulation)
At start of hold 580 °C	1.1	0.8	0.5	0.5
2 h – 580 °C	1.1	0.9	1.0	1.0
12 h – 580 °C	1.3	1.2	1.3	1.5

fraction of dispersoids increases depending on the initial local segregation profile as shown in Fig. 3b. As demonstrated in Fig. 3c, the dispersoids are initially rich in Mn with a Mn/Fe ratio of 20–30. This is consistent with the TEM/EDS measurements of 16.3. As the homogenization treatment is extended to 2 h at 580 °C, two important changes can be observed. First, the Mn/Fe ratio for the dispersoids decreases significantly and shows a gradient from left to right with the ratio decreasing from 9 to 2. This compares to the experimental measurements which showed an average ratio of 6.6. Second, it is possible to see the formation of small DFZ beside the constituent particle, i.e. the region from ≈8 to 9.5 μm. Upon further holding at 580 °C for 12 or 24 h, the Mn/Fe ratio of the dispersoids decreases to ≈4 (viz. experimental value of 4.6) and the width of the DFZ increases.

One of the advantages of the model is the ability to interrogate it to determine parameters that are almost impossible to determine from experiments. Fig. 4a and b show the flux of Mn and Fe atoms (positive numbers indicate motion from left to right and negative values are for motion from right to left). Here it can be seen that the Mn atoms always diffuse from left to right (to the constituent particle). On the other hand, the behaviour of the Fe flux is very different. For the case of 0 min at 580 °C (i.e. the end of the heating), one can see that there is a flux of Fe atoms leaving the constituent particle and diffusing into the primary aluminum dendrite. For the cases of 30 min and 2 h at 580 °C, the flux has penetrated further into the dendrite (with the resulting decrease in Mn/Fe ratio of the dispersoids shown in Fig. 3c) but in the latter case, one can observe that the flux out of the constituent particle is decreasing. Finally, for the cases of 12 and 24 h at 580 °C, the flux has now reversed and Fe along with Mn is now moving back to the constituent particle and the composition of the dispersoids has stabilized with a Mn/Fe ratio of ≈4.

The diffusion of Mn (and Fe at long times) to the constituent particles leads to an increase in their volume fraction. The model predicts that their volume fraction increases from an initial value of 0.8% to 1.2% after 12 h at 580 °C and there is a corresponding change in the Mn/Fe ratio of the constituent particles from 0.5 to 1.5 as reported in Table 2. The change in the volume fraction and composition of the constituent particles is dominated by the mass transport of Mn from the primary aluminum to constituent particles, i.e. it can be seen that the flux of Mn to the particles is much larger than that for Fe as shown in Fig. 4. The results from the model were validated experimentally using image analysis to measure the volume fraction and the EPMA results to characterize the Mn/Fe ratio. Table 2 summarizes the experimental and simulation results for the volume fraction and Mn/Fe ratio for the evolution of the constituent particles during homogenization at 580 °C. Here, it can be observed that there is very good agreement between the model results and the experimental measurements for the Mn/Fe ratio and reasonable agreement for the volume fraction noting that it is challenging to experimentally measure small volume fractions of particles using image analysis, i.e. it is very dependent on the threshold used to separate the particles from the matrix.

In summary, the evolution of the microstructure during homogenization is driven by a number of factors including the initial distribution of Mn and Fe after solidification (the primary aluminum dendrites are highly supersaturated in Mn), the dependence of the dispersoid chemical potential on Fe content which drives Fe to the dispersoids, the higher diffusivity of Fe compared to Mn (the diffusion coefficient for Fe at 580 °C is almost 10 times faster than Mn), the solubility of Fe in the aluminum (which limits mass transport) and the interaction between Mn and Fe on the free energy of the solid solution. The complex interaction between these different factors illustrates the need for a model which can be used to predict the important characteristics of the dispersoid precipitation reaction and the changes in the constituent particles. Having established a model which has been validated by experiments, future work involves a study on the effect of alloy chemistry (primarily the Mn and Fe contents) and homogenization conditions to examine new approaches to producing the desired microstructure consisting of a homogeneous distribution of dispersoids with high volume fraction and small size to maximize the Zener pinning pressure so as to minimize recrystallization during extrusion.

Acknowledgements

The authors would like to thank Dr. Xiang Wang from the Canadian Centre for Electron Microscopy at McMaster University for assistance with the TEM work. The financial support of NSERC and Rio Tinto Aluminium are gratefully acknowledged.

References

[1] L.J. Colley, M.A. Wells, W.J. Poole, Can. Met. Quart. 53 (2014) 125–137.
[2] M. Cai, J.D. Robson, G.W. Lorimer, Scr. Mater. 57 (2007) 603–606.
[3] C. Liu, H. Azizi-Alizamini, N.C. Parson, W.J. Poole, Mater. Sci. Forum 794–796 (2014) 1199–1204.
[4] L. Lodgaard, N. Ryum, Mat. Sci. Eng. A 283 (1–2) (2000) 144–152.
[5] C. Poletti, C. Wojcik, C. Sommitsch, Metall. Mater. Trans. A 44 (2013) 1577–1586.
[6] J. Chen, W.J. Poole, N.C. Parson, Mater. Sci. Forum 794–796 (2014) 1127–1132.
[7] K. Strobel, M.A. Easton, L. Sweet, M.J. Couper, J.F. Nie, Mater. Trans. 52 (2011) 914–919.
[8] B. Milkereit, M.J. Starink, Mater. Des. 76 (2015) 117–129.
[9] P. Priya, D.R. Johnson, J.M. Krane, Metall. Mater. Trans. A 47A (2016) 4625–4639.
[10] M. Cooper, Acta Crystall. 23 (1967) 1106–1107.
[11] M. Cooper, K. Robinson, Acta Crystall. 20 (1966) 614–617.
[12] K. Sugiyama, N. Kaji, K. Hiraga, Acta Crystall. Sect. C. Crystall. Struct. Comm. 54 (1998) 445–447.
[13] J.M. Dowling, J.W. Martin, Acta Metall. 24 (1976) 1147–1153.
[14] K. Strobel, M.A. Easton, L. Sweet, M.J. Couper, J.F. Nie, Mater. Trans. 52 (2011) 914–919.
[15] A.L. Dons, J. Light. Met. 1 (2001) 133–149.
[16] A.L. Dons, Aluminium 78 (2002) 839–842.
[17] Q. Du, W.J. Poole, M.A. Wells, N.C. Parson, Acta Mater. 61 (13) (2013) 4961–4973.
[18] H. Demers, N. Poirier-Demers, A.R. Couture, D. Joly, M. Guilmain, N. de Jonge, D. Drouin, Scanning 33 (2011) 135–146.
[19] J.L. Pouchou, F. Pichoir, in: J.T. Armstrong (Ed.), Microbeam Analysis 1985, pp. 104–106.
[20] M.N. Gungor, Metall. Mater. Trans. A 20 (1989) 2529–2533.
[21] M. Ganesan, D. Dye, P.D. Lee, Metall. Mater. Trans. A 36 (2005) 2191–2204.
[22] Q. Du, W.J. Poole, M.A. Wells, Acta Mater. 60 (9) (2012) 3830–3839.
[23] Q. Du, A. Jacot, Acta Mater. 53 (2005) 3479–3493.